

Fracto-emission in lanthanum-based metallic glass microwires under quasi-static tensile loading

Amit Banerjee, Chenchen Jiang, Lokesh Lohiya, Yong Yang, and Yang Lu

Citation: *Journal of Applied Physics* **119**, 155102 (2016); doi: 10.1063/1.4946824

View online: <http://dx.doi.org/10.1063/1.4946824>

View Table of Contents: <http://scitation.aip.org/content/aip/journal/jap/119/15?ver=pdfcov>

Published by the *AIP Publishing*

Articles you may be interested in

[Stable fracture of a malleable Zr-based bulk metallic glass](#)

J. Appl. Phys. **112**, 103533 (2012); 10.1063/1.4767327

[The deformation units in metallic glasses revealed by stress-induced localized glass transition](#)

J. Appl. Phys. **111**, 113522 (2012); 10.1063/1.4728207

[Mechanical behavior of a Zr-based metallic glass at elevated temperature under high strain rate](#)

J. Appl. Phys. **108**, 033511 (2010); 10.1063/1.3467779

[Local strain behavior of bulk metallic glasses under tension studied by in situ x-ray diffraction](#)

Appl. Phys. Lett. **94**, 011911 (2009); 10.1063/1.3064136

[Tensile behavior of bulk metallic glasses by in situ x-ray diffraction](#)

Appl. Phys. Lett. **91**, 081913 (2007); 10.1063/1.2773945

A promotional banner for AIP Applied Physics Reviews. The background is a dark blue gradient with a bright light source on the right, creating a lens flare effect. On the left, there is a small image of the journal cover for 'Applied Physics Reviews', which features a 3D diagram of a layered structure. The main text 'NEW Special Topic Sections' is in large, white, bold, sans-serif font. Below this, the text 'NOW ONLINE' is in yellow, followed by 'Lithium Niobate Properties and Applications: Reviews of Emerging Trends' in white. The AIP logo and 'Applied Physics Reviews' text are in the bottom right corner.

NEW Special Topic Sections

NOW ONLINE
Lithium Niobate Properties and Applications:
Reviews of Emerging Trends

AIP Applied Physics
Reviews

Fracto-emission in lanthanum-based metallic glass microwires under quasi-static tensile loading

Amit Banerjee,^{1,2} Chenchen Jiang,^{1,3} Lokesh Lohiya,¹ Yong Yang,^{1,3} and Yang Lu^{1,2,3,4,a)}

¹Department of Mechanical and Biomedical Engineering, City University of Hong Kong,

83 Tat Chee Avenue, Kowloon, Hong Kong

²Centre of Super-Diamond and Advanced Films (COSDAF), City University of Hong Kong,

83 Tat Chee Avenue, Kowloon, Hong Kong

³Centre for Advanced Structural Materials (CASM), City University of Hong Kong,

83 Tat Chee Avenue, Kowloon, Hong Kong

⁴Shenzhen Research Institute, City University of Hong Kong, Shenzhen 518057, China

(Received 26 January 2016; accepted 31 March 2016; published online 19 April 2016)

Plastic deformation in metallic glasses is highly localized and often associated with shear banding, which may cause momentary release of heat upon fracture. Here, we report an explosive fracture phenomenon associated with momentary (~ 10 ms) light emission (*flash*) in Lanthanum-based (LaAlNi) metallic glass microwires (dia. ~ 50 μm) under quasi-static tensile loading. The load-displacement data as well as the visual information of the tensile deformation process were acquired through an *in situ* measurement set-up, which clearly showed nonlinear stress (σ)–strain (ϵ) curves prior to yielding and also captured the occurrence of the *flash* at high fracture stresses (~ 1 GPa). Through the postmortem fractographic analysis, it can be revealed that the fracto-emission upon quasi-static loading could be mainly attributed to the localized adiabatic work accumulated at a very large elastic strain confined within the microscale sample volume, followed by a localized high temperature rise up to ~ 1000 K at the fracture surface through localized energy dissipation. Our findings suggest that the La-based metallic glass microwires could be useful for energetic microchips, micro-ignition devices, and other functional applications. *Published by AIP Publishing.*

[<http://dx.doi.org/10.1063/1.4946824>]

I. INTRODUCTION

Amorphous metal alloys, produced by rapid quenching from their liquid mixture, are known for having extraordinary mechanical strength that makes them suitable for many practical applications.^{1–4} Atoms in such metallic systems remain in a *glassy* state as their arrangement lacks in a long-range translational symmetry, unlike in usual crystalline metals. This makes their mechanical behavior quite different from normal metals having crystalline lattice structures, which can facilitate dislocation movement under stress, making them comparatively *soft* and ductile. Metallic glasses (MGs), on the other hand, are *hard*, relatively brittle,⁵ and high in mechanical strength.⁶ As the atoms lack in the long-range periodicity in their arrangement, the thermo-kinetic behavior of the atoms (or a significant portion of them) in the glassy form is similar to liquid.⁷ However, depending on the quenching rate and other effects during the fabrication, localized short-range correlation in atomic arrangement, which gives rise to solid like behavior, is easy to find.^{8,9} Therefore, solid-like (crystalline) and liquid-like (amorphous) zones are often observed side-by-side in the atomic scale through high resolution transmission electron microscopy.¹⁰ Such microscopic structure is responsible for making the mechanical behavior of metallic glasses viscoelastic in nature.^{11–13}

Lack of structural dislocation in a metallic glass prevents significant plastic deformation, and the mechanics is usually confined to elastic (*anelastic*) regime. The plastic deformation is usually confined to extremely localized areas (*plastic zones*) in the material, giving rise to an adiabatic compression that causes a high degree of local temperature rise, occasionally leading to melting of the material,^{14,15} resulting in a catastrophic failure. The entire mechanical energy accumulated during the deformation process suddenly releases during this short lived and localized plastic deformation, causing a significant part of the mechanical energy to dissipate in the form of heat. If the temperature rise is high enough, it can stimulate a flash emission of visible radiation, and subsequent burning or pyrolysis (in the presence and absence of air, respectively) of the burnable components of the material, as was demonstrated by Gilbert *et al.*¹⁶ in Zirconium based *bulk* (size ~ 10 mm) metallic glass through *impact* loading/fracture (with very high strain-rate). Here, we report a light emitting fracture mechanism in Lanthanum-based metallic glass material at much *lower length-scale* (~ 50 μm) and at relatively much *lower strain-rate*. In the present experiment, MG microwires are quasi-statically (strain-rate $\sim 10^{-4}$ s^{-1}) tensioned through an *in situ* microtest set-up (see Section II) until fracture, which has been observed to be associated with the emission of visible flashes of light (fracto-emission). From the stress (σ)–strain (ϵ) curves acquired under linear loading, we also observed nonlinearity from a very small amount of strain (ϵ). We show that this behavior can be attributed to linear

^{a)}Author to whom correspondence should be addressed. Electronic mail: yanglu@cityu.edu.hk

viscoelasticity through a phenomenological model. Through fractographic analysis with high-resolution scanning electron microscopy and elemental analysis through energy dispersive X-ray spectroscopy (EDS), we propose a mechanism for the fracto-emission observed in our samples.

II. SAMPLES AND EXPERIMENTAL PROCEDURES

The metallic glass (MG) microwire samples (dia. 40–80 μm) used in this work are fabricated by rapid quenching of an alloy of Lanthanum, Aluminum, and Nickel in 5:3:2 atomic proportions from their liquid mixture. The chemical composition of the metallic glass is evaluated through the energy dispersive x-ray spectroscopy (EDS) studies carried out on the MG microwires, which reaffirmed the composition to be approximately $\text{La}_{50}\text{Al}_{30}\text{Ni}_{20}$ (in atomic %). X-ray diffraction (XRD) studies on the MG microwires are carried out to confirm the amorphous nature of the material.

In situ tensile mechanical studies are carried out through GatanTM Deben Microtest 200 micro-tensile-test system (Figure 1(a)) mounted under a high-resolution optical camera, and subsequently inside a scanning electron microscope (FEITM Quanta FEG-SEM). This machine is equipped with a 200 N load-cell (L) with force sensitivity ~ 1 mN. The MG microwire samples are mounted on the two flat jaws (J_1 and J_2 ; Figure 1(a)), which moves apart from each other with precise and controllable speed through a precision motor (M), producing controlled tensile deformation. The corresponding force generation is sensed and measured by the load-cell. The samples are usually mounted directly on the movable jaws (J_1 and J_2) through screw-clamping for bulk samples (~ 1 mm). However, to ensure firm clamping on the MG microwires (and to avoid the possibility of sliding), we adopt a technique, where the two ends of the metallic glass microwires (length 2–3.5 mm, diameter 45–80 μm) are attached on two copper plates (through soldering and superglue), which are then mounted and clamped on the two “jaws” of the Microtest machine (Figure 1(a)). The motor-speed, data acquisition time, etc., are controlled through the software, and

the load-displacement data are collected through the load-cell attached with the machine.

The force-displacement data sets for the MG microwire samples are collected at different strain-rates (α). The motor-speed is kept unchanged (0.1 mm/min), whereas the length of the MG microwires is varied, giving rise to different values of α from sample to sample. During a particular study, α is kept unchanged. In order to convert the load–displacement data, the dimensions of the MG microwire samples are carefully measured. The areas of cross-section of the microwires are calculated by measuring their average diameter from their magnified images (captured through optical and electron microscopes).

III. RESULTS

The microtensile testing setup along with the MG microwire sample mounting process is depicted in Figure 1(a) (see Section II). Figure 1(b) shows a representative result acquired from one of the tensile tests ($\alpha \approx 4.52 \times 10^{-4} \text{ s}^{-1}$) with the corresponding stress-strain data. The stress-strain curve ($\sigma - \epsilon$) in Figure 1(b) shows an interesting nonlinear behavior. The $\sigma - \epsilon$ curve begins with an apparent linear regime (cf. the straight-line L1) at very low ϵ value, followed by a significantly curved region (cf. the curve C) at intermediate ϵ value, and finally saturates to another seemingly linear regime (represented by the line L2), before it finally fails at $\epsilon_u \approx 2\%$ and at ultimate tensile strength $\sigma_u \sim 1$ GPa. This nature of the $\sigma - \epsilon$ relation is repeatedly observed in the MG microwires of different lengths and at different α values, and we propose that it can be explained through a phenomenological linear viscoelastic model, a schematic of which is shown in the inset of Figure 1(b) (to be discussed later). The deviation from linearity after the linear regime (L1) may apparently indicate an early setting in of plasticity; however, this can be explained by linear viscoelastic flow behavior, owing to the low flow activation energy.

The fracture process in the MG microwire samples is observed to be sudden, catastrophic failure as normally

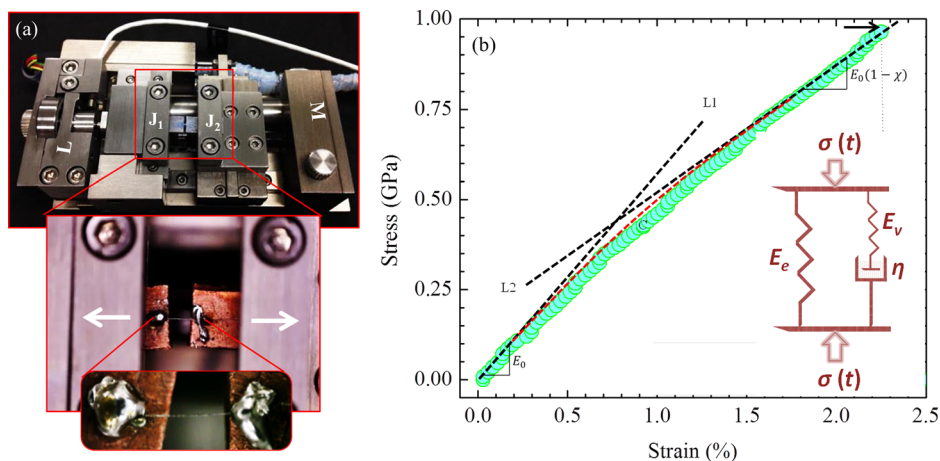


FIG. 1. (a) A photograph of the micro-tensile system and the experimental arrangement adopted during the present study, (b) a typical stress-strain curve for the metallic glass microwires showing the nonlinear behavior (the filled circles represent actual experimental data, and the dashed lines (L1, L2) and the curve (c) are used for representing different regimes). The continuous curve fitted on the data shows the fitting of Equation (2). The inset shows a schematic diagram of the phenomenological viscoelastic model, consisting of a Hookean linear spring and a Maxwellian linear viscoelastic arm in parallel combination, adopted to explain the nonlinear behavior of the stress-strain curve.

observed in brittle materials. At the fracture point, indicated by the arrow in Figure 1(b), the event of light flash emission occurs (Figure 2). We observed that the whole fracture process happens within the duration of one frame of the *in situ* video (see supplementary material,¹⁷ movie captured by an optical camera; frame time ~ 40 ms), as shown in Figures 2(a)–I–2(a)–III, where the fracture process is observed to take place in frame-II. Frame-I and frame-III are the adjacent frames of the *in situ* video exactly before and after the fracture process. The emission of a flash of visible light is evident from Figure 2(a)–II. This indicates that the duration of this entire explosive fracture process is ~ 80 ms; however, this is only the upper limit of the duration, and the actual process probably takes even less time.¹⁶

Due to the lack of a periodic lattice structure, a pervasive plastic deformation mechanism across the entire material facilitated by usual dislocation dynamics cannot take place inside the material of the MG microwires. Plastic deformation process is short-lived and is subjected to a high degree of spatial confinement (namely, plastic zone). Extremely localized plastic deformation near the fracture point generates heat as the deformation effectively becomes an adiabatic process, suddenly releasing the stored elastic energy, even at low strain-rate owing to this spatial

confinement. Low thermal conductance (k) of the MG material assists this localized heating process to take place. Local temperature rise (ΔT) in the material inside the plastic zone can be roughly calculated by the following relation:¹⁸

$$\Delta T = (1.414(1 - \nu^2)K_c\sigma_u\sqrt{V})/(E_0\sqrt{\rho Ck}),$$

where ν , K_c , σ_u , E_0 , ρ , and C represents the Poisson's ratio, fracture toughness, yield strength, effective Young's modulus, density, and heat capacity of the material of the MG microwire, respectively, and V is the maximum speed of crack propagation, which is comparable ($\sim 92\%$) to the shear wave speed (V_s).¹⁸ Using experimentally measured values of ρ , E_0 , σ_u with typical values of K_c ($\sim 1 \text{ MPa m}^{1/2}$), k ($\sim 5 \text{ W m K}^{-1}$), σ_u ($\sim 1 \text{ GPa}$), V_s ($\sim 10^3 \text{ ms}^{-1}$, velocity of sound in solid material), and C ($\sim 10^3 \text{ J kg}^{-1} \text{ K}^{-1}$), ΔT is roughly estimated to be $\sim 1000 \text{ K}$. This temperature rise within such a small time-scale ($\sim 10 \text{ ms}$) causes the explosive fracture to be accompanied by the emission of a flash of visible light, as observed in Figure 2(a)–II. This sudden high temperature rise causes pyrolytic change in the material if the experiments are carried out in a vacuum or in a non-reactive environment; however in such an environment condition, the temperature rise is followed by burning of the burnable components. The emission spectrum is red-shifted (i.e., predominant emission in infra-red regime) in the vacuum condition as opposed to a white light emission in the environmental condition.¹⁶ This process could be interpreted into three steps: (i) high temperature rises due to localized adiabatic work at large elastic strain, and subsequently (ii) oxidation reaction (burning) of the material with environment upon fracture, followed by (iii) even higher temperature rises causing local melting of fracture surface.

The SEM image in Figure 2(b) shows an MG microwire (tested inside the SEM) immediately after the fracture. It is evident from the magnified image that the fractured MG microwire does not show any significant *necking* near the fracture area, strongly suggesting the absence of a substantial plastic deformation even until fracture. This observation also suggests that the deviation of the $\sigma - \epsilon$ behavior from linearity is not due to plastic deformation.

IV. DISCUSSIONS

A. Phenomenological model for the non-linear stress-strain behavior

The experiments are repeated on the multiple MG microwire samples at different α to verify the flash emission as well as to investigate the nonlinear behavior of the $\sigma - \epsilon$ curves represented in Figure 1(b). We propose that the nonlinear behavior of the $\sigma - \epsilon$ curves (shown in Figure 1(b)) can be interpreted purely in terms of linear viscoelasticity, without invoking the assumption of nonlinear elasticity or plasticity. We adopt a phenomenological viscoelastic model,¹³ as shown in the schematic diagram in the inset of Figure 1(b), to explain the nonlinear $\sigma - \epsilon$ behavior. The model assumes that the material of the MG microwire consists of two parts, one of which is a linear elastic material and is represented by the Hookean spring (E_e), whereas the other part is a linear viscoelastic

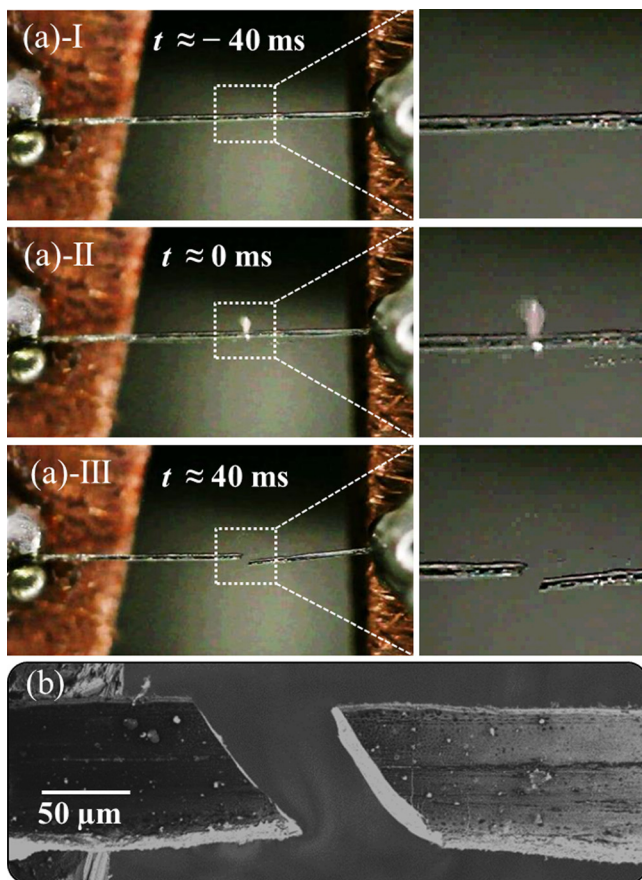


FIG. 2. (a) Fracto-emission in the MG microwire under uniform quasistatic tensile loading; I, II, and III represent three consecutive frames (frame time ~ 40 ms), with frame-II bearing the light emitting fracture event with a visible flash of light, (b) SEM micrograph of a fractured MG microwire studied inside the SEM, showing no significant *necking* in or around the fracture location, suggesting the absence of long-range plastic deformation.

material depicted by the Maxwellian arm consisting of a linear Hookean spring (E_v) and a *dashpot* behaving as a Newtonian viscous fluid (η). The elastic and viscoelastic parts are combined with each other, and they can be separately identified only in the atomic scale, as shown by Wang *et al.*¹⁰ If the volume fraction of the viscoelastic part be χ ($0 < \chi < 1$), then E_e and E_v can be expressed in terms of an overall effective elastic modulus (E_0) as $E_e = (1 - \chi)E_0$ and $E_v = \chi E_0$, and the effective viscosity can be expressed as $\eta_{eff} = \chi\eta$.

The corresponding phenomenological equation for adopted model can be summarized in the following equation:¹³

$$\sigma(t) = (1 - \chi)E_0\epsilon(t) - \frac{\eta}{E_0}\dot{\sigma} + \eta\dot{\epsilon} \quad (1)$$

(“dot” mark over the variables represents first order time derivative).

Rearranging terms and taking Laplace transformation of Equation (1) (see supplementary material¹⁷)

$$\bar{\sigma} \left(1 + \frac{\eta s}{E_0} \right) = [(1 - \chi)E_0 + \eta s]\bar{\epsilon} + \left(\frac{\eta}{E_0}\sigma_0 - \eta\epsilon_0 \right),$$

where $\bar{\sigma}$ and $\bar{\epsilon}$ are, respectively, the Laplace transformation of σ and ϵ , and σ_0 and ϵ_0 are their initial values (at $t = 0$). Since $\epsilon = \alpha t$, the Laplace transformation $\bar{\epsilon} = \frac{\alpha}{s}$ (where s is the Laplace space variable). Inserting this in the above equation, and subsequently taking an inverse Laplace transformation, we arrive at the solution of the differential equation (1), as given by the following $\sigma - \epsilon$ relation (see supplementary material¹⁷):

$$\sigma = E_0\epsilon \left[1 - \chi \left\{ \frac{1 - e^{-\beta}}{\beta} \right\} \right], \quad (2)$$

where $\beta = \frac{E_0\alpha}{\eta}$.

Note: in the limiting cases, the following linear relations between stress and strain will hold:

$$\lim_{\beta \rightarrow 0} \sigma = E_0\epsilon; \quad \lim_{\beta \rightarrow \infty} \sigma = E_0(1 - \chi)\epsilon.$$

Since $E_0, \alpha, \eta > 0$, $\beta \rightarrow 0$, or $\beta \rightarrow \infty$ essentially imply $\epsilon \rightarrow 0$ and $\epsilon \rightarrow \infty$, therefore, these limiting cases: (i) explain the linear nature of the $\sigma - \epsilon$ curves at very low and high ϵ values, as well as predict the in-between curvature at intermediate values of ϵ (Equation (2)), and (ii) imply that the initial linear slope of the stress-strain curve would be E_0 , and for a large value of strain, the curve should asymptotically converge to the slope of $E_0(1 - \chi)$.

The experimental $\sigma - \epsilon$ curves are fitted with Equation (2) (cf. the continuous curve fitted with the experimental data in Figure 1(b)) for extracting the values of fitting parameters: E_0 , χ , and η_{eff} for best fit curves. The values of E_0 and χ are also compared well with the limiting case conditions discussed above. The value of E_0 is observed to be within 43.5–78.0 GPa, whereas the values of η_{eff} lie within 243–684 GPa s.

B. Post-mortem analysis of the fracture surface

High-resolution SEM images captured during post-mortem analysis of the fracture surface bears the evidence of sudden high temperature rise, as discussed in the context of Figure 2(a). The overall microstructure of the fracture surface is shown in the SEM image of Figure 3(a). Upon magnification (Figure 3(b)), several spherical metallic beads are observed on the fracture surface. One such spherical metal particle is shown in Figure 3(b), with a magnified image in the inset. The spherical shape of these particles suggests melting and subsequent solidification of the material, indicating a sudden temperature rise above the melting point of the MG material. The vein-pattern observed in the so called *mirror zone* of the fracture surface (Figures 3(a) and 3(b)) is typically found in the fracture surface of glassy materials. These vein-patterns bear the signature of liquid like flow occurring inside the MG material. The local temperature rise changes the local density (as well as the viscosity) of the material, and intermixing of two liquids with different densities

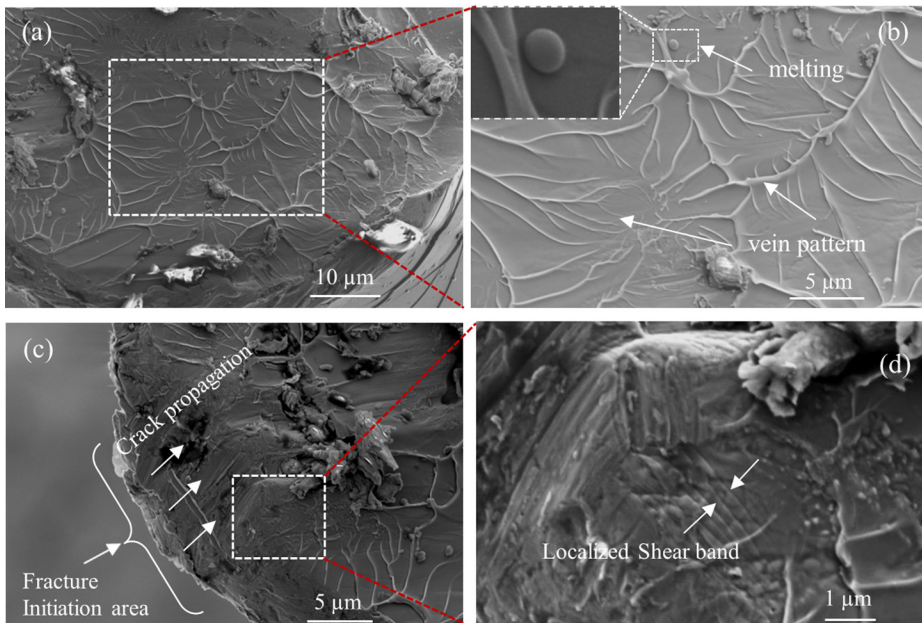


FIG. 3. Microstructure of the fracture surface captured through SEM showing the (a) overall microstructure of the fracture surface with vein-patterns, (b) existence of spherical beads as an indication of melting and subsequent solidification of the material due to sudden temperature rise; the inset shows the magnified image of one such bead, (c) crack initiation area and propagation direction, and the magnified image showing (d) localized shear-bands.

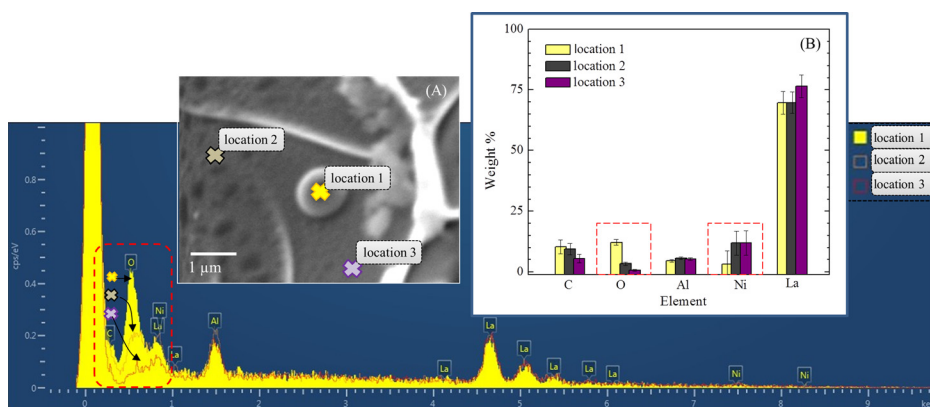


FIG. 4. The main panel shows the EDS spectra captured from different locations on the fracture surface as indicated in inset A. Inset B shows the weight % of different elements at the locations indicated in inset A.

is responsible for producing such fractal like patterns, due to Rayleigh-Taylor instability. The SEM image in Figure 3(c) shows the area in the MG microwire, where from the crack is initiated; the direction of crack propagation is also indicated by the arrows. By zooming in the area inside the dotted rectangle in Figure 3(c), we also observe some localized shear bands (SEM image of Figure 3(d)) of size ~ 200 nm, indicating a confined plastic work, which we argued earlier to be responsible for the explosive light emitting fracture.

C. Local elemental analysis on the fracture surface

The occurrence of the fracto-emission for metallic glass wires in quasi-static deformation is typically not expected. However, the EDS analysis (main panel of Figure 4) carried out at multiple locations (marked by x in inset A in Figure 4) on the fracture surface provides useful information suggesting a plausible mechanism. The elemental analysis of the spherical beads (namely, location 1) by EDS shows that the beads contain a significant amount of oxygen (~ 12 wt. %, as opposed to 1–3.5 wt. % outside but on the fracture surface (locations 2 and 3), and almost no oxygen away from the fracture surface), indicating that an oxidation reaction (burning) at high temperature has taken place (see, inset B in Figure 4, for weight % of different elements inside the spherical bead, and outside). We attribute the burning mainly to the relatively low burning point of Lanthanum, which readily burns in the presence of oxygen (at $\sim 150^\circ\text{C}$) to produce lanthanum (III) oxide.¹⁹ To further confirm this, we performed additional tensile tests with similar straining rates on other types of metallic glass microwires/ribbons without La phase, such as CoFeBSiNb and FeB, and did not observe such fracto-emission phenomenon. In addition, the small sample volume of the microwires provides the larger (fracture) surface to volume ratio, which further assists the burning with air exposure. On the other hand, the EDS analysis of the spherical beads revealed that they contain significantly less amount of Ni (inset B in Figure 4), compared to the original composition of the material and the neighboring areas on the fracture surface. This implies that the final temperature rise upon the fracto-emission is sufficient to melt La and Al, however is insufficient to melt Ni. Considering that the melting-points of the constituents La, Al, and Ni are 1193, 934, and 1726 K, respectively, this important observation

imposes a lower and an upper bound on the actual temperature rise. The theoretical calculation suggesting approximate local temperature rise of ~ 1000 K is therefore justifiable, as the melting points of Al and La are around 1000 K, whereas that of Ni is much higher, about 1700 K.

V. CONCLUSION

In summary, we demonstrate that Lanthanum-based metallic glass microwires underwent an explosive fracto-emission process under a quasi-static tensile loading process, followed by a sharp and localized temperature rise up to ~ 1000 K. Experimental evidences of the temperature rise and a mechanism to explain the fracto-emission phenomenon have been investigated and proposed, respectively. Potential applications of this property of La-based metallic glass could be in controllable micro-heating/ignition sources, which can be potentially useful in microsurgery, micro-chemical-reactors, and other functional devices.

ACKNOWLEDGMENTS

This work was supported by the Research Grants Council of the Hong Kong Special Administrative Region, China under the Project Nos. CityU 138813, CityU 11209914, and CityU 9042066, and the National Natural Science Foundation of China (NSFC) Grant No. 51301147. A.B. thanks the ITT-GTA postdoctoral scheme of City University of Hong Kong.

The authors declare no competing financial interests.

¹W. K. Jun, R. H. Willens, and P. Duwez, "Non-crystalline structure in solidified gold-silicon alloys," *Nature* **187**, 869–870 (1960).

²W. L. Johnson, A. Inoue, and C. T. Liu, *Bulk Metallic Glasses*, MRS Proceedings Vol. 554 (Cambridge University Press, 1999).

³W. H. Wang, C. Dong, and C. H. Shek, "Bulk metallic glasses," *Mater. Sci. Eng., R* **44**, 45–89 (2004).

⁴A. Inoue, *Bulk Amorphous Alloys: Practical Characteristics and Applications* (Trans Tech Publications, 1999).

⁵B. Sarac and J. Schroers, "Designing tensile ductility in metallic glasses," *Nat. Commun.* **4**, 2158 (2013).

⁶Y. B. Wang *et al.*, "Ultrahigh-strength submicron-sized metallic glass wires," *Scr. Mater.* **84–85**, 27–30 (2014).

⁷Q. Wang, Y. Yang, H. Jiang, C. T. Liu, H. H. Ruan, and J. Lu, "Superior tensile ductility in bulk metallic glass with gradient amorphous structure," *Sci. Rep.* **4**, 4757 (2014).

⁸A. Hirata, P. Guan, T. Fujita, Y. Hirotsu, A. Inoue, A. R. Yavari, T. Sakurai, and M. Chen, "Direct observation of local atomic order in a metallic glass," *Nat. Mater.* **10**, 28–33 (2011).

- ⁹H. Wagner, D. Bedorf, S. Küchemann, M. Schwabe, B. Zhang, W. Arnold, and K. Samwer, "Local elastic properties of a metallic glass," *Nat. Mater.* **10**, 439–442 (2011).
- ¹⁰Q. Wang, C. T. Liu, Y. Yang, J. B. Liu, Y. D. Dong, and J. Lu, "The atomic-scale mechanism for the enhanced glass-forming-ability of a Cu-Zr based bulk metallic glass with minor element additions," *Sci. Rep.* **4**, 4648 (2014).
- ¹¹J. C. Ye, J. Lu, C. T. Liu, Q. Wang, and Y. Yang, "Atomistic free-volume zones and inelastic deformation of metallic glasses," *Nat. Mater.* **9**, 619–623 (2010).
- ¹²N. Nagendra, U. Ramamurty, T. T. Goh, and Y. Li, "Effect of crystallinity on the impact toughness of a La-based bulk metallic glass," *Acta Mater.* **48**, 2603–2615 (2000).
- ¹³L. S. Huo, J. Ma, H. B. Ke, H. Y. Bai, D. Q. Zhao, and W. H. Wang, "The deformation units in metallic glasses revealed by stress-induced localized glass transition," *J. Appl. Phys.* **111**, 113522 (2012).
- ¹⁴J. J. Lewandowski and A. L. Greer, "Temperature rise at shear bands in metallic glasses," *Nat. Mater.* **5**, 15–18 (2006).
- ¹⁵Y. Zhang, N. A. Stelmashenko, Z. H. Barber, W. H. Wang, J. J. Lewandowski, and A. L. Greer, "Local temperature rises during mechanical testing of metallic glasses," *J. Mater. Res.* **22**, 419–427 (2007).
- ¹⁶C. J. Gilbert, J. W. Ager III, V. Schroeder, R. O. Ritchie, J. P. Lloyd, and J. R. Graham, "Light emission during fracture of a Zr–Ti–Ni–Cu–Be bulk metallic glass," *Appl. Phys. Lett.* **74**, 3809–3811 (1999).
- ¹⁷See supplementary material at <http://dx.doi.org/10.1063/1.4946824> for the movie showing the fracto-emission of a La-based metallic glass microwire upon fracture under quasi-static tensile loading (video is played in real time; "flash" occurred at ~54 s) and the detailed calculation of the stress-strain relationship.
- ¹⁸G. Wang, D. Q. Zhao, H. Y. Bai, M. X. Pan, A. L. Xia, B. S. Han, X. K. Xi, Y. Wu, and W. H. Wang, "Nanoscale periodic morphologies on the fracture surface of brittle metallic glasses," *Phys. Rev. Lett.* **98**, 235501 (2007).
- ¹⁹P. Patnaik, *Handbook of Inorganic Chemical Compounds* (McGraw-Hill, 2003), pp. 444–446, ISBN: 0070494398.